Toggling of seismicity by the 1997 Kagoshima earthquake couplet: A demonstration of time-dependent stress transfer

Shinji Toda

Active Fault Research Center, Geological Survey of Japan, Agency of Industrial Science and Technology, Tsukuba, Japan

Ross Stein

U.S. Geological Survey, Menlo Park, California, USA

[1]   Two $M \sim 6$ well-recorded strike-slip earthquakes struck just 4 km and 48 days apart in Kagoshima prefecture, Japan, in 1997, providing an opportunity to study earthquake interaction. Aftershocks are abundant where the Coulomb stress is calculated to have been increased by the first event, and they abruptly stop where the stress is dropped by the second event. This ability of the main shocks to toggle seismicity on and off argues that static stress changes play a major role in exciting aftershocks, whereas the dynamic Coulomb stresses, which should only promote seismicity, appear to play a secondary role. If true, the net stress changes from a sequence of earthquakes might be expected to govern the subsequent seismicity distribution. However, adding the stress changes from the two Kagoshima events does not fully capture the ensuing seismicity, such as its rate change, temporal decay, or migration away from the ends of the ruptures. We therefore implement a stress transfer model that incorporates rate/state friction, in which seismicity is treated as a sequence of independent nucleation events that are dependent on the fault slip, slip rate, and elapsed time since the last event. The model reproduces the temporal response of seismicity to successive stress changes, including toggling, decay, and aftershock migration. Nevertheless, the match of observed to predicted seismicity is quite imperfect, due perhaps to inadequate knowledge of several model parameters. However, to demonstrate the potential of this approach, we build a probabilistic forecast of larger earthquakes on the expected rate of small aftershocks, taking advantage of the large statistical sample the small shocks afford. Not surprisingly, such probabilities are highly time- and location-dependent: During the first decade after the main shocks, the seismicity rate and the chance of successive large shocks are about an order of magnitude higher than the background rate and are concentrated exclusively in the stress triggering zones.   INDEX TERMS: 7209 Seismology: Earthquake dynamics and mechanics; 7223 Seismology: Seismic hazard assessment and prediction; 7230 Seismology: Seismicity and seismotectonics; 7260 Seismology: Theory and modeling; KEYWORDS: Coulomb stress, stress triggering, seismicity

1.   Introduction

[2]   A principal tenet of the Coulomb hypothesis is that stress increases promote, and decreases inhibit, fault failure. However, stress changes alone cannot explain the time behavior of seismicity, such as the universally observed Omori decay of aftershocks, or the commonly seen migration of seismicity from the fault. When the Coulomb hypothesis is modified to incorporate the effects of rate/state friction [Dieterich, 1994], a sudden Coulomb stress increase causes a large increase in seismicity rate, but decays back toward its initial rate inversely with time.

A sudden stress drop causes the seismicity rate to plummet, also recovering toward its initial rate. Thus, in what we refer to as "rate/state stress transfer," the evolution of seismicity depends not only on the stress change and the static friction coefficient, but also on the background seismicity rate, a fault constitutive parameter, and either the fault stressing rate or an aftershock decay period. At the cost of these additional often uncertain parameters, rate/state stress transfer offers the prospect of more accurate seismicity forecasts.

[3]   Some progress has been achieved in demonstrating rate/state stress transfer in seismicity. Aftershocks located off the main fault rupture have proven the most useful tests of the concept. Among the weaknesses in such studies, however, is the difficulty of measuring seismicity rate declines, which
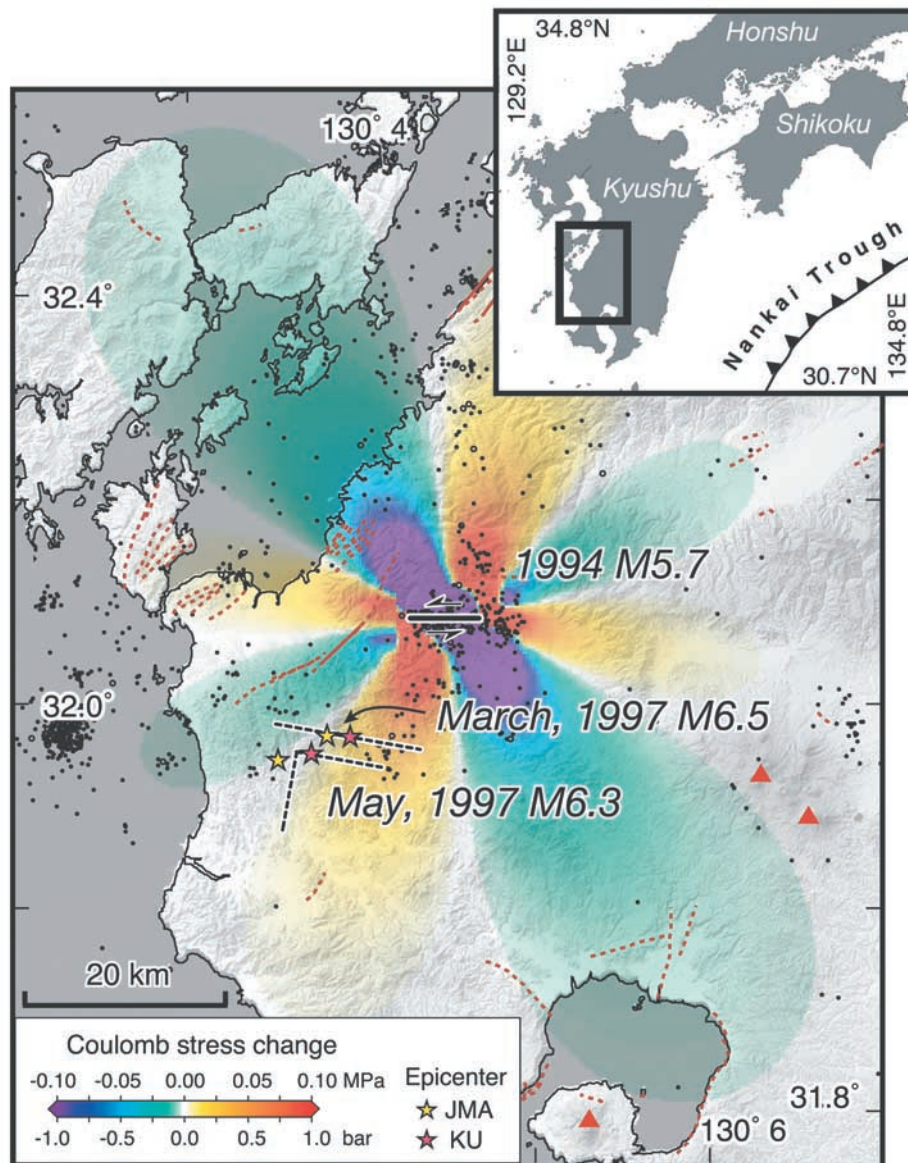
Figure 1.   Site of the 13 February 1994 M_{JMA} = 5.7 shock Kagoshima shock (fault shown as solid black line) and 1997 Kagoshima earthquake sequence (faults shown as dashed black lines) in southwest Japan, together with January 1990 to February 1997 JMA $M \geq 2.2$ seismicity. Other active faults are red (dashed where inferred); active volcanoes are red triangles [*Earthquake Research Committee*, 1998]. The Coulomb stress field resulting from the 1994 shock resolved on left-lateral strike-slip faults is superimposed in color. Receiver faults are assumed to strike 280°, dip 90°, and rake 0° with a friction coefficient, $\mu' = 0.8$. Source parameters for the 1994 shock are from the Harvard CMT solution ($M = 5.4$, strike 89°, dip 89°, rake −1°, latitude/longitude 32.03°/130.33°) assuming a 7.3 × 7.3 km patch with 0.28 m of slip). For $\mu' = 0.4$, failure is promoted by 0.25 bar only on the east half of the March 1997 fault.

requires a high background seismicity rate before the perturbing earthquake. Earthquakes in which stress decreases, or "stress shadows," have been associated with seismicity rate decreases include the 1989 $M = 6.9$ Loma Prieta [*Reasenberg and Simpson*, 1997; *Parsons et al.*, 1999; *Stein*, 1999], 1906 $M = 7.9$ San Francisco [*Harris and Simpson*, 1998], 1995 $M = 6.9$ Kobe [*Toda et al.*, 1998], 1992 $M = 7.3$ Landers [*Wyss and Wiemer*, 2000], and 1983 $M = 6.7$ Coalinga earthquake [*Toda and Stein*, 2002] events.

[4]   A more convincing demonstration of rate/state stress transfer demands a case in which an off-fault region is

subjected to alternating stress increases and decreases, or "toggling" stress changes. In the 1997 Kagoshima sequence, the 26 March $M = 6.1$ and 13 May $M = 6.0$ main shocks (M_{JMA} 6.5 and 6.3, respectively) struck close together in time and space (Figure 1). The geometrical simplicity of the earthquakes, coupled with the quality of the seismic, strong motion, and geodetic data provide an opportunity to subject rate/state stress transfer to a more powerful test. We will argue that the common practice of adding the Coulomb stress of two or more successive earthquakes to predict the resulting seismicity pattern [e.g., *Stein et al.*, 1997; *Nalbant et al.*,
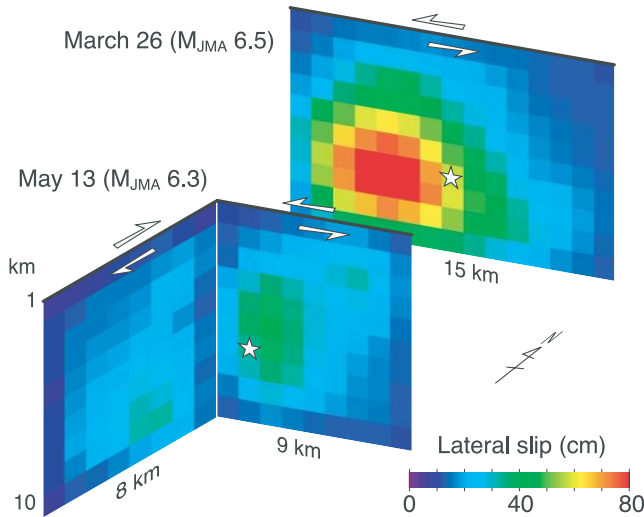
Figure 2. Variable slip model of *Horikawa* [2001] for the 1997 couplet. The March and May sources have been separated to make the March slip visible in this perspective.

1998; *Hubert-Ferrari et al.*, 2000] is inferior to a rate/state stress transfer model.

[5] The Kagoshima couplet is also valuable for inferring whether the static or dynamic stress change is principally responsible for the subsequent local seismicity rates. Unlike the static stress change, the dynamic stress oscillates between positive and negative values, and so no region will experience only a dynamic stress drop. Although both static and dynamic stress changes can explain seismicity increases near source, a sustained seismicity rate drop can be only explained by the static stress change.

2. Data

[6] The 1997 earthquakes struck on three unmapped faults in a region of Kyushu Island with few known active faults and a low rate of historical seismicity. The Philippine Sea Plate subducts beneath southern Kyushu along the Nankai Trough at a rate of ∼40 mm yr^{-1} (Figure 1, inset). Unlike sites adjacent to the Nankai Trough, southern Kyushu is undergoing NW-SE extension [*Sagiya et al.*, 2000]. Most shallow earthquakes are strike slip, and several active volcanoes and calderas align with a N-S trending volcanic front. No large destructive earthquake has struck within 75 km of the 1997 Kagoshima epicenters since records were kept starting in AD 679; the largest shock within 30 km is a 1994 $M_{JMA} = 5.7$ event that occurred 15 km to the northeast [*Earthquake Research Committee*, 1998; *Miyamachi et al.*, 1999] (Figure 1). The 1997 sequence produced left-lateral slip on two east striking planes and right-lateral slip on a north striking plane, with the ruptures oriented about 45° to the azimuth of the extensional strain. The Harvard CMT main shock focal mechanisms indicate nearly pure strike-slip faulting on vertical faults. From strong motion analysis, *Horikawa* [2001] found a seismic moment of 1.6×10^{18} N m for the 26 March event, with unilateral westward or bilateral rupture propagation. For the 13 May main shock, he found a moment of 1.0×10^{18} N m on two orthogonal faults, with

rupture initiating near their junction. Variable slip models for both events from *Horikawa* [2001] are shown in Figure 2. The general features are consistent with independent InSAR and continuous GPS analysis of the March event by *Fujiwara et al.* [1998]. The asperity model of *Miyake et al.* [1999] also resembles Horikawa's slip distributions.

[7] To study the response of seismicity to stress changes imparted by the Kagoshima shocks, one must measure the background seismicity rate before 26 March 1997 above the minimum magnitude of completeness, M_c (the magnitude at which the catalog is complete for a given period). If earthquakes with magnitudes below M_c were included, there would be an apparent increase in seismicity following the main shock, because seismic stations that are typically added after a large main shock enhance detection [*Matthews and Reasenberg*, 1988; *Wiemer and Wyss*, 2000]. Both the national Japan Meteorological Agency (JMA) and local Kagoshima University (KU) [*Miyamachi et al.*, 1999] catalogs are available (Figure 3). *Miyamachi et al.* [1999] relo-
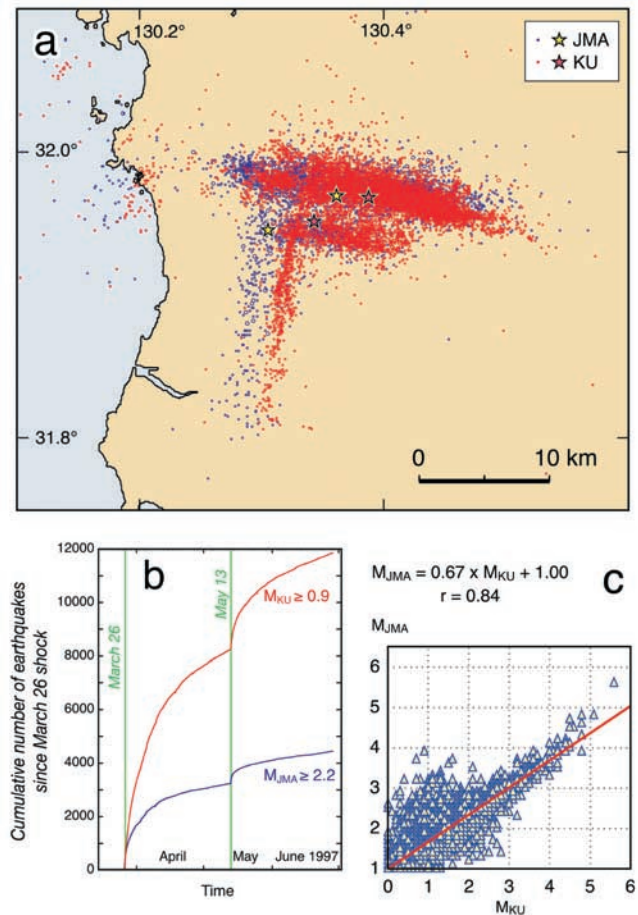
Figure 3. (a) Seismicity during the 96-day period starting 26 March from the JMA (blue) and Kagoshima University (KU, red) catalogs. (b) Cumulative number of earthquakes as a function of time, at the magnitude of completeness, for the JMA and Kagoshima University catalogs for the same period. (c) Regression of JMA and KU magnitudes, needed to estimate the background rate from both catalogs. JMA and KU catalog events separated by <1 min and <5 km were assumed to be the same shocks.
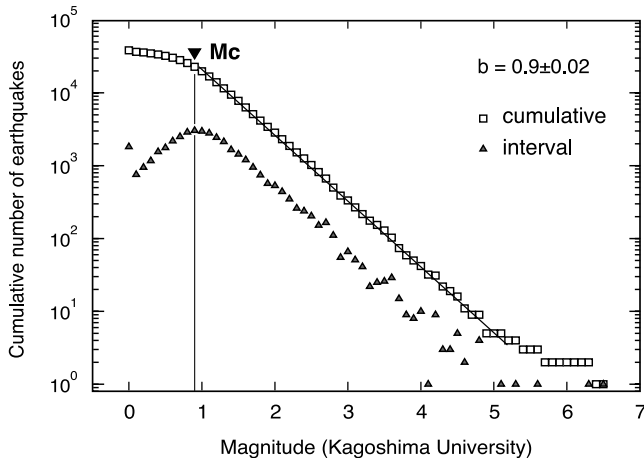
Figure 4. Maximum likelihood solution for the minimum magnitude of completeness, M_c, for the Kagoshima University catalog for March 1996 to March 2001, calculated using ZMAP of *Wiemer* [2001]. The b value is for $0.9 \geq M \geq 5.0$.

cated the Kagoshima University catalog events in a 3-D P wave velocity model inverted from travel times of 14 stations; $M_c = 0.9$ during March 1996 to March 2001 (Figure 4). JMA augmented its network in October 1994, after which $M_c = 2.2$. While the lower M_c and improved locations for the Kagoshima University data make it a better choice, $M_{KU} = 0.9$ is roughly equivalent to $M_{JMA} = 1.6$ (Figure 3c), so the disparity in the number of earthquakes between the catalogs is smaller than it would appear. Differences in epicenter locations between two catalogs are significant in the west of the source regions and moderate in the east. As shown in the separations of two main shock epicenters between the JMA and KU catalog (Figure 3a), aftershock locations in the KU catalog also systematically shift to the east by 2−4 km from the JMA locations due to the different P wave velocity model. We thus use the KU catalog except when estimating the background seismicity rate, for which both catalogs are used.

3. Coulomb Stress Changes

[8]   The static Coulomb stress change caused by a main shock ΔCFF is calculated by

$$\Delta \text{CFF} = \Delta\tau + \mu(\Delta\sigma_n + \Delta p) \qquad (1)$$

where $\Delta\tau$ is the shear stress change on a give fault plane (positive in the direction of fault slip), $\Delta\sigma_n$ is the fault-normal stress change (positive for unclamping), μ is the coefficient of friction, Δp is the pore pressure change within the fault.

[9]   We make all calculations in an elastic half-space [*Okada*, 1992] and use the apparent friction μ' which precludes distinguishing the effect of the pore pressure change from the normal stress change (unclamping/unclamping) [*Cocco and Rice*, 2002] and is given by

$$\Delta \text{CFF} = \Delta\tau + \mu'\Delta\sigma_n \qquad (2)$$

3.1. Main Shock Triggering

[10]   We first examine the interaction of the three largest shocks. We calculate that the 1994 $M_{JMA} = 5.7$ earthquake

brought the March 1997 rupture 0.2−0.5 bar (0.02−0.05 MPa) closer to Coulomb failure, if the friction coefficient is as high as 0.8. This inference is consistent with the presence of off-fault aftershocks in the northern and southern triggering lobes of the 1994 shock; seismicity extends to the future 1997 fault plane (Figure 1). If fault friction were low, however, the effects of the 1994 shock would be negligible at the 1997 epicenters. *Parsons et al.* [1999] found that seismicity associated with faults with little cumulative slip is favored more by unclamping than shear, and thus youthful or low slip rate faults may exhibit higher fault friction. The absence of a mapped fault in the 1997 events would suggest little cumulative slip, and so a high value of apparent friction ($\mu' \sim 0.8$) may indeed be appropriate.

[11]   The triggering of the May earthquake by the March event does not provide support for the Coulomb hypothesis, in part because which of the two orthogonal faults ruptured first in the May event is unknown. The stress change associated with the March rupture is resolved on the May faults in Figure 5. The shear stress change is negative except near the ground surface, whereas the normal stress unclamps both faults within 3 km of their junction, as previously reported by *Horikawa* [2001]. The May hypocenter appears to lie on the western edge of the E-W fault (Kagoshima University location). Only if the more strongly unclamped N-S fault ruptured first would the E-W rupture be subsequently unclamped. Although *Miyake et al.* [1999] found that the N-S fault ruptured several seconds before the E-W rupture, *Horikawa* [2001] concluded the opposite, so rendering triggering conclusions ambiguous.

3.2. Aftershock Triggering

[12]   Our principal focus is not on the several main shocks, but on the thousands of off-fault aftershocks, because they provide a large statistical sample, and are far enough from the source faults that their stress change is well determined. Figures 6a−6c show the Coulomb stress change associated with the March rupture, together with seismicity during the intervening 48 days before the May shock. The stress change associated with the May rupture, with the ensuing 48 days of seismicity, is shown in Figures 6d−6f. The cumulative stress changes imparted by both earthquakes are shown in Figures 6g−6i. The three columns plot different assumed receiver fault plane orientations and friction coefficients. Focal mechanisms of $M \geq 3$ aftershocks appear consistent with the assumption of north striking or east striking vertical faults (Figure 7). We exclude from consideration earthquakes within 3 km of the fault ruptures (comprising 75% of the total), which we regard as arising from small-scale slip discontinuities and secondary fault fractures that are not represented by the smooth, planar slip model. For both the March and May stress changes, regions of concentrated off-fault aftershocks correspond to sites of calculated stress increase, and off-fault aftershocks are rare in the stress shadows.

[13]   Although the correspondence between off-fault stress change and seismicity is good, there are features in the seismicity that cannot be explained by the stress changes alone. In Figure 8, we plot the daily rate of earthquakes in three off-fault boxes, marked A−C in Figure 6. These sites, although arbitrarily selected, all experienced calculated stress changes more than ±0.3 bars during each main shock,
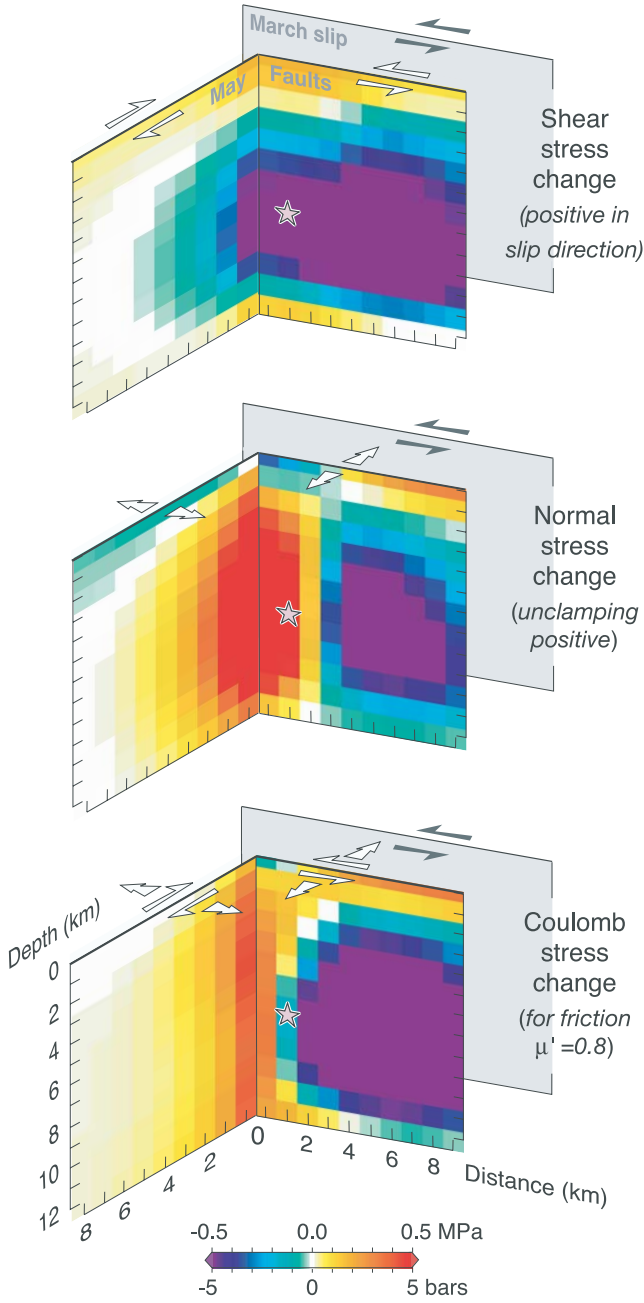
Stress change resolved on May rupture planes

Figure 5. Perspective view of stress imparted by the March main shock resolved on the planes that ruptured in May. Slip direction is represented by the black arrows; stress components are represented by the white arrows. The May hypocenter given by Kagoshima University is shown as a star.

and contain enough aftershocks to test their responses to stress change. Here we use $\mu' = 0.8$ on the basis of the inferred 1994–1997 main shock triggering, the youth of the faults, and the correspondence in Figure 6 (right two columns). Note that in most cases, the seismicity rate changes by orders of magnitude after each main shock, whereas the stress change is never more than 4 bars. Boxes

A and B were subjected to roughly the same net stress change (1.8 and 1.9 bars, respectively), yet the post-May seismicity rate is five times higher in box B (3.0 shocks d^{-1}) than in box A (0.6 shock d^{-1}). Neither these disparities, nor the Omori-like inverse time decay in the seismicity rate after the March event in box A, can be explained by adding the static Coulomb stress changes, encouraging us to seek a more comprehensive model.

4. Rate/State Stress Transfer

[14] To consider successive stress changes associated with multiple main shocks, we use the expression for seismicity rate R as a function of the state variable γ under a tectonic secular shear stressing rate $\dot{\tau}_r$ from *Dieterich* [1994]. Under constant shear stressing rate, the state variable reaches the steady state, and is expressed as

$$\gamma_0 = \frac{1}{\dot{\tau}_r} \qquad (3)$$

At steady state, the seismicity rate R is equivalent to the background reference rate r because R is calculated from the following simple relation

$$R = \frac{r}{\gamma \dot{\tau}_r} \qquad (4)$$

In the absence of a large stress perturbation, the seismicity rate is assumed constant. A sudden stress step ΔCFF alters the seismicity rate. The state variable γ_{n-1} before the stress step changes to a new value γ_n

$$\gamma_n = \gamma_{n-1} \exp\left(\frac{-\Delta CFF}{A\sigma}\right) \qquad (5)$$

where $A\sigma$ is the constitutive parameter times the total normal stress. To seek the seismicity at the time of the stress step, we substitute the new state variable in (4). An important element of rate/state friction theory is a nonlinear dependence of the time to instability on stress change. The effect of the stress increase on a fault due to a nearby main shock is to cause γ to drop, so the fault slips at a higher rate, causing a higher rate of seismicity. Conversely, a sudden stress drop causes γ to jump, lowering the rate of seismicity. However, the seismicity rate change is transient and recovers, corresponding to gradual evolution of γ, which for the next time step is given by

$$\gamma_{n+1} = \left[\gamma_n - \frac{1}{\dot{\tau}_r}\right] \exp\left[\frac{-\Delta t \dot{\tau}_r}{A\sigma}\right] + \frac{1}{\dot{\tau}_r} \qquad (6)$$

where Δt is a time increment used to recalculate γ at each time step. The duration of the transient is inversely proportional to the fault stress rate $\dot{\tau}_r$. Thus, given sufficient time (e.g., decades to centuries), the effect of all but the largest of earthquakes disappears.

[15] A key feature of rate/state stress transfer is that the value of γ before each shock plays a profound role on the effect of the coseismic stress change: the higher the rate of seismicity at the time of a stress step, the more strongly it will be amplified by the stress change
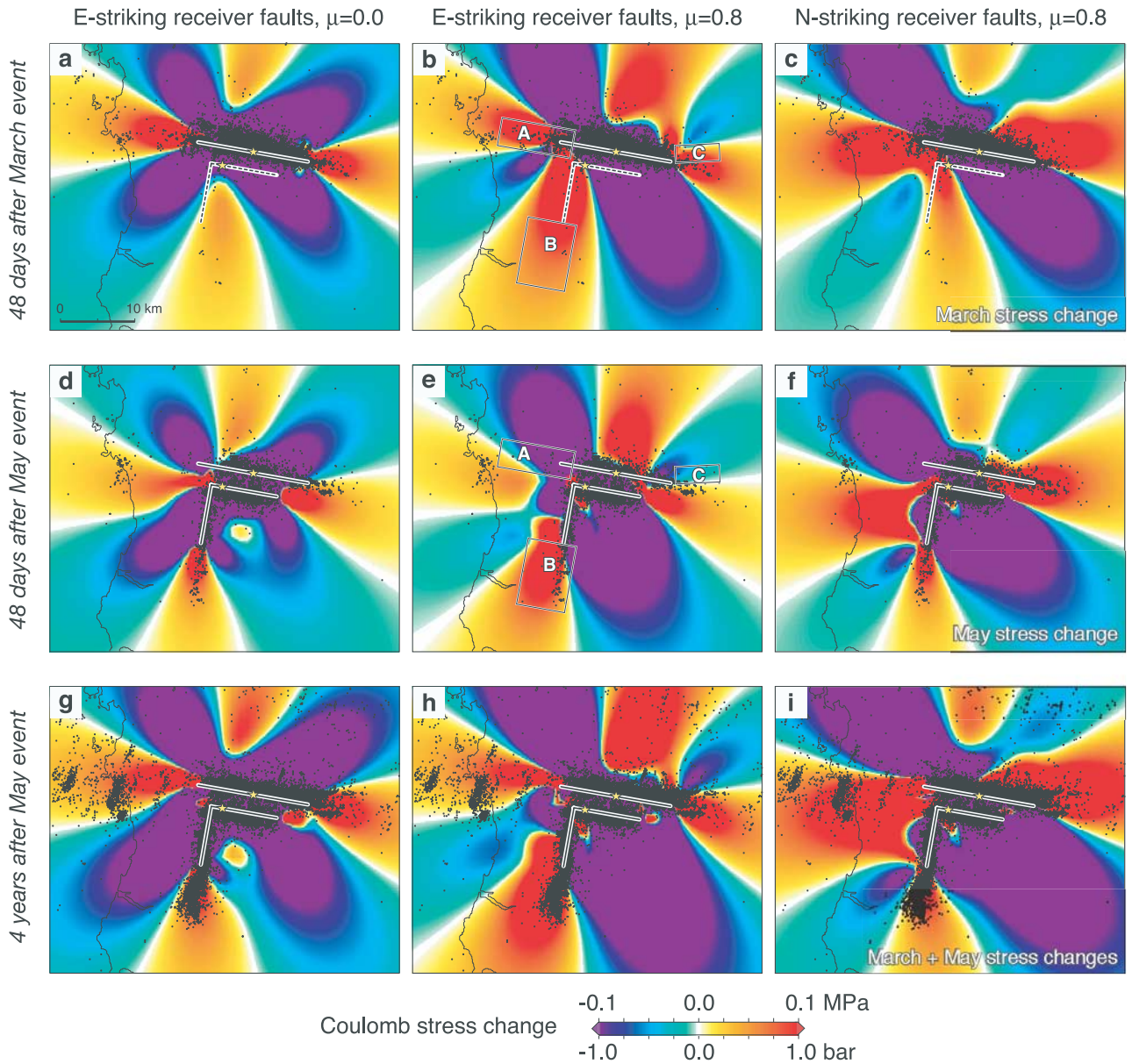
Figure 6. Aftershocks from the Kagoshima University catalog relocated by *Miyamachi et al.* [1999] superimposed on coseismic stress changes at 5 km depth for the (a–c) March and (d–f) May main shocks; both are 48-day periods. Figures 6b and 6e show boxes for the seismicity time series plotted in Figure 8. The combined stress changes and the full 4 years of post-13 May shocks are shown in Figures 6g–6i. Different assumed receiver faults and friction coefficients are represented by the columns.

(Figure 9), In Figure 9a, for example, a 1-bar stress step can increase the seismicity rate by a factor of 10 or 100 depending on the preceding rate [*Marone*, 2002; *Toda et al.*, 2002]. Further, if the steady background rate r is low, the stress changes have a muted effect on seismicity. Thus, as apparent at Kagoshima, two sites that sustain the same net increase in stress can produce different increases in seismicity rate.

4.1. Parameter Values

[16] To evaluate terms in the equations, r is estimated from the background seismicity rate before the March main

shock assuming that r had attained a steady state. Then the Coulomb stress change is calculated for the March and May main shocks on a 1×1 km grid. The parameter, $A\sigma$ (constitutive parameter times the normal stress) describes the instantaneous response of friction to a step change in slip speed. We assume $A\sigma = 0.4$ bar, based on the stress-change dependence of seismicity rate at the site of the 1995 Kobe earthquake [*Toda et al.*, 1998], another large strike-slip event in inland Japan. Similar estimates have been determined by *Guatteri et al.* [2001] for the Kobe shock ($A\sigma = 0.6$ bar), and by *Belardinelli et al.* [1999] for the 1980 $M = 6.9$ Irpinia, Italy, earthquake ($A\sigma = 0.8$–0.9 bar). Given
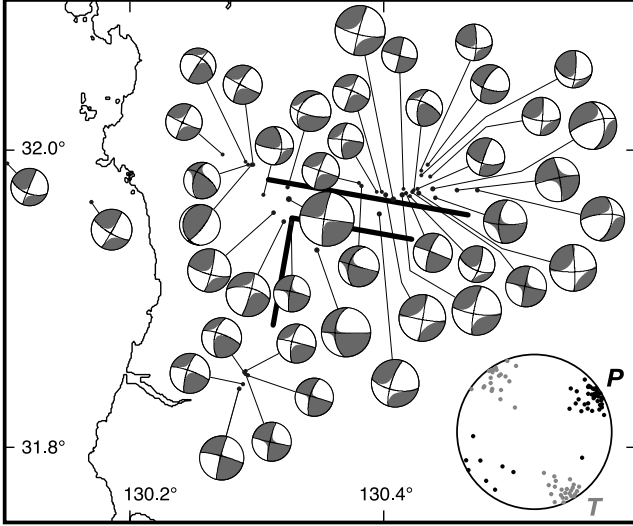
Figure 7. All well-determined focal mechanisms for $M \geq 3$ shocks, as determined by the F net broadband network during March 1997 to March 2001 [*NIED Staff*, 2001]. The majority of both on-fault and off-fault shocks exhibit nodal planes parallel to the rupture planes of the main ruptures. The stress field (lower right inset) is consistent with left-lateral slip on east striking planes or right-lateral slip on north striking faults.
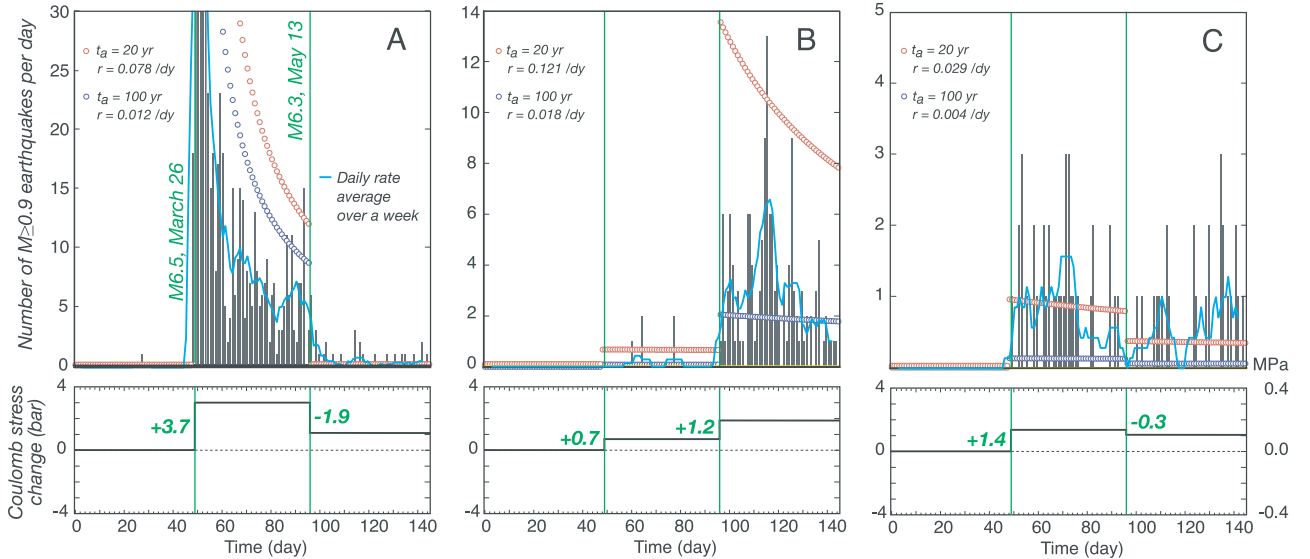
includes only one year before 26 March 1997 shock complete to $M_c = 0.9$. From this we estimate a spatially uniform rate of 0.09 km^{-2} yr^{-1} (162 events in the 1820 km^2 region), which we consider a lower bound because of uncertainty in M_c for so short a period. The JMA catalog can also supply an estimate of the background rate, after conversion to equivalent KU magnitudes. There were 181 $M_{JMA} \geq 2.2$ shocks in the study area during the 2.5-year period, October 1994 to March 1997. From the comparison between JMA and KU catalogs (Figure 3c), $M_{JMA} = 0.67 M_{KU} + 1.00$. So $M_{JMA} = 2.2$ corresponds to $M_{KU} = 1.8$. Because $b = 0.9$ (Figure 4), $N_{M=0.9} = N_{M=1.8} b \times 10^{(1.8-0.9)} = 1438$ earthquakes. The background rate of $M_{KU} \geq 0.9$ would then be 0.3 km^{-2} yr^{-1}, 3.5 times higher than the more direct estimate based on a briefer period. Since many of the JMA shocks occurred in the 1994 rupture zone, the JMA rate is less representative of the region as a whole, and so we consider it an upper bound. We use this range, together with the along-fault aftershock decay for the March and May main shocks, to estimate the aftershock duration $t_a = 20-100$ years (Figure 10). Although consistent with independent assessments of 23 ± 8 years for Kobe [*Toda et al.*, 1998] and 35 ± 8 years for the North Anatolia fault [*Parsons et al.*, 2000], none of these durations is well determined. Since $\dot{\tau}_r = A\sigma/t_a$ [*Dieterich*, 1994], $\dot{\tau}_r = 0.004-0.02$ bar yr^{-1}, a reasonable value given the observed (deviatoric) shear strain rate of $0.10-0.15 \times 10^{-6}$ yr^{-1} [*Sagiya et al.*, 2000].

4.2. Model Comparison With Seismicity Time Series

[18] Although sensitive to the aftershock duration t_a, the rate/state stress transfer model captures the observed time-dependent evolution of seismicity in the selected boxes fairly well (Figure 8, top), and it certainly does better than the stress changes alone (Figure 8, bottom). In box A, just

laboratory measurements of A [*Dieterich*, 1994], such values of $A\sigma$ would imply a low effective normal stress σ (5–20 bars).

[17] The background seismicity rate r before the Kagoshima sequence is uncertain because the seismic catalogs have limited periods at the requisite magnitude of completion. The Kagoshima University catalog


Figure 8. Observed and modeled seismicity time series for the boxed regions shown in Figure 6. Daily seismicity rates, smoothed with a running 7-day window, are blue. (top) Note that the seismicity rate scale differs for each box. (bottom) Each time series is the calculated Coulomb stress history for $\mu' = 0.8$. The background seismicity rates r used vary as a function of box size; the estimated rate is 2.5×10^{-4} km^{-2} d^{-1}. The range in aftershock duration t_a is shown in Figure 10.
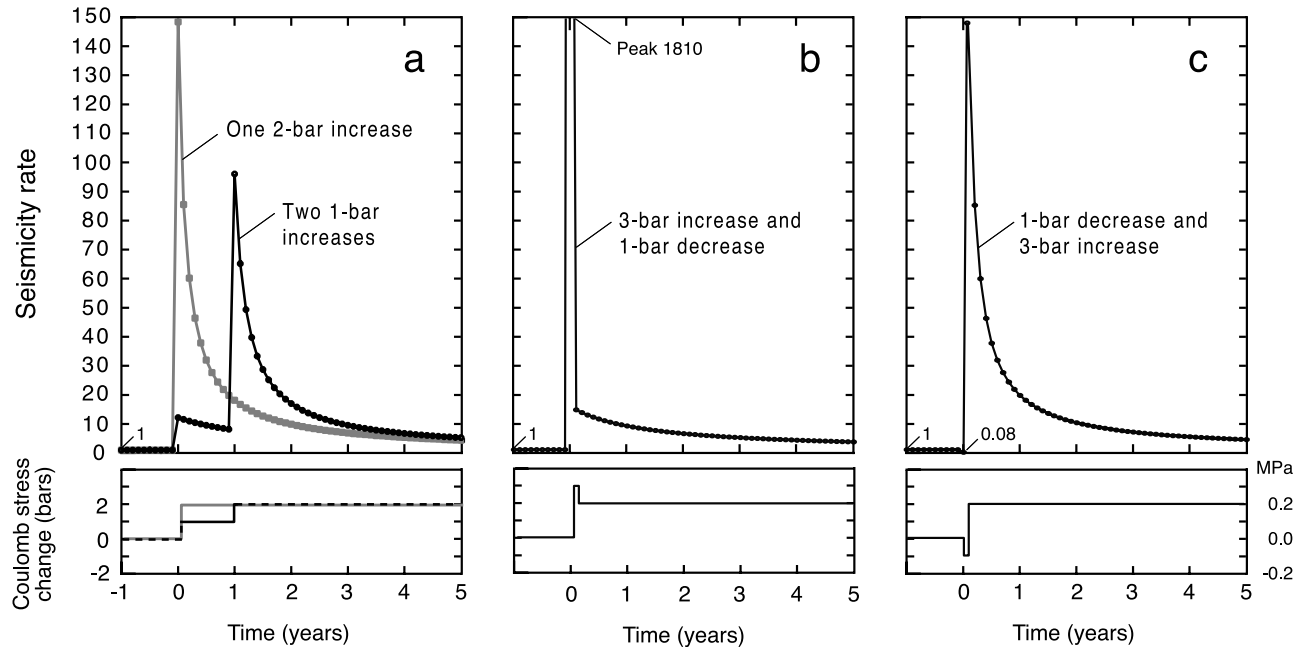
Figure 9. Response of seismicity to a sequence of stress changes, as predicted by rate/state stress transfer (equations (3)−(6)). The background rate, r, is set to 1, t_a= 20 years and $A\sigma$ = 0.4, 0.1-year time increments are used. The net stress change is 2 bars in all four cases (a−c), but the seismicity rate depends on the stressing history. Note a 1-bar stress change increases the immediately preceding rate by a factor of 10.

off the western end of the March rupture, the observed inverse time decay in seismicity resembles the rate/state model. Box B, just off the south end of the May rupture, was subjected to a 1.2-bar stress increase, and is associated

with increase in seismicity rate by more than an order of magnitude. Both the seismicity rate jump and ensuing decay are fit by the rate/state model with t_a between 20 and 100 years. Box C is in the trigger zone off the east end of
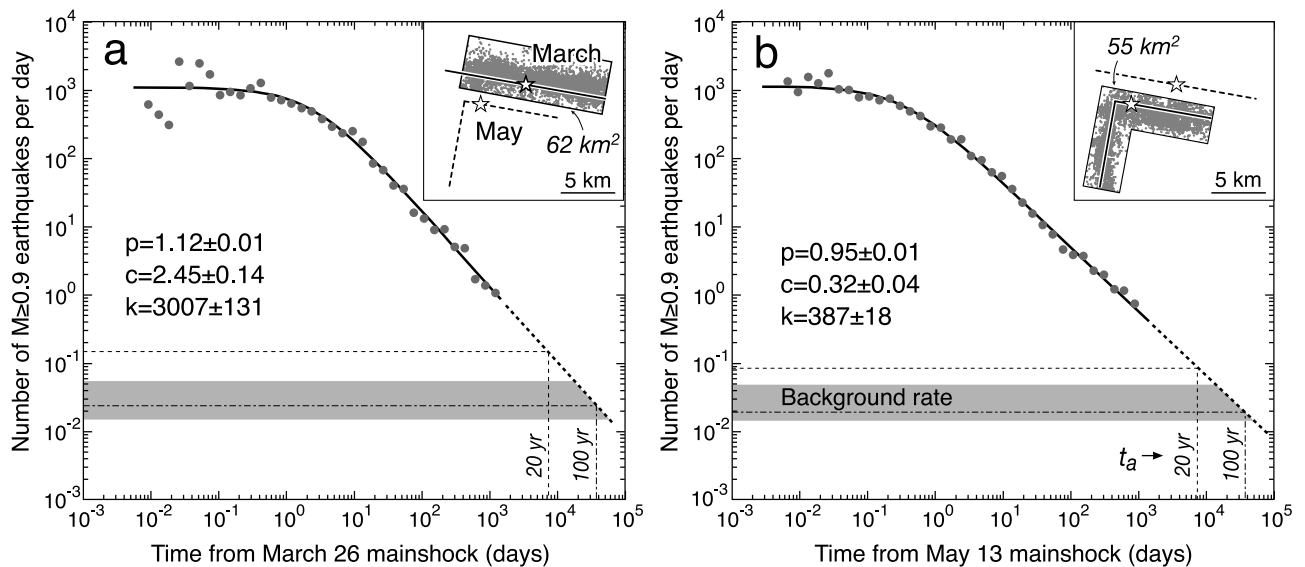
Figure 10. Observed aftershock rate (dots) as a function of time for the 26 March and 13 May shocks, fitted to a modified Omori decay function (solid line), $N(t) = k/(t + c)^P$. Aftershocks and the associated fault ruptures are shown in the inset maps, and the bounds on the estimated background rate are shown gray horizontal bands. The lower bound comes from the 1996 rate in the Kagoshima University (KU) catalog; the upper bound is from the 1994−1996 rate in the JMA catalog, after conversion to equivalent KU magnitudes. The inferred aftershock duration t_a corresponds to the time when the projected aftershock rate (heavy dashed line) decays to the background rate.
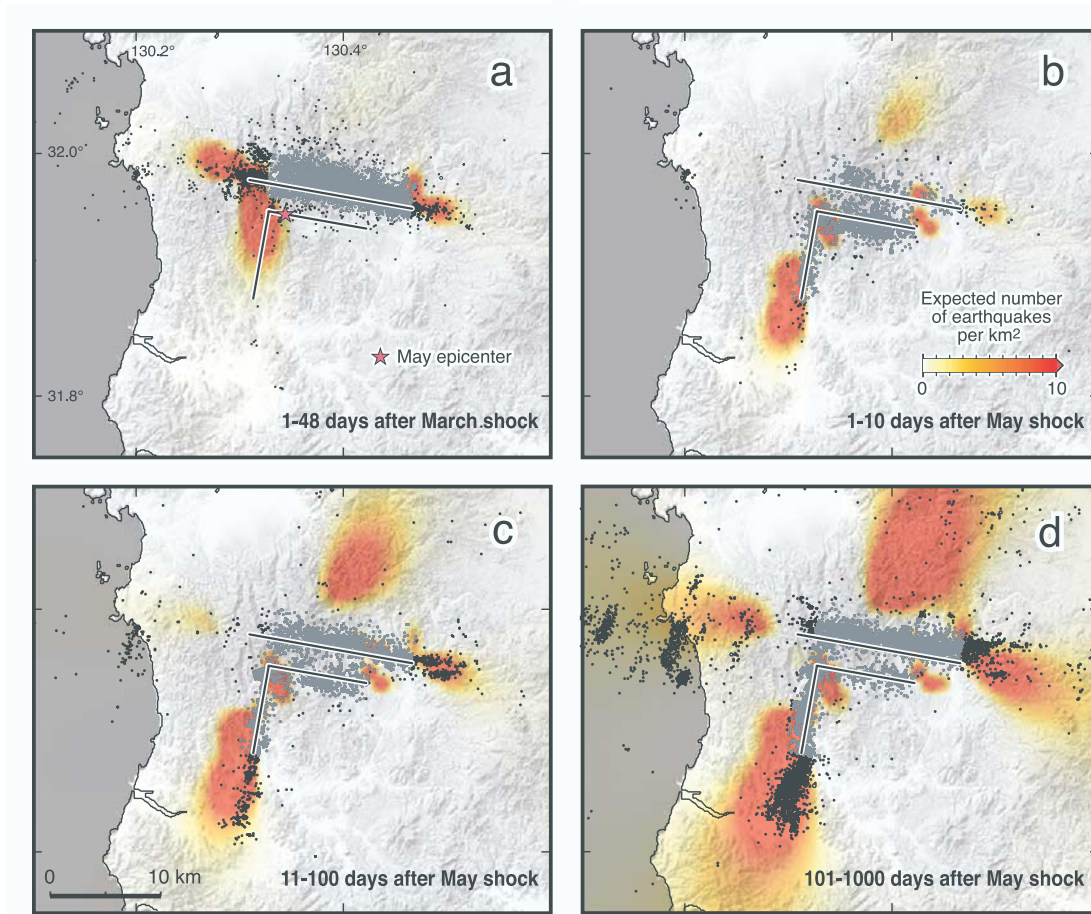
Figure 11. Observed seismicity, superimposed on the expected number of earthquakes calculated by rate/state stress transfer (for east striking receiver faults with $\mu' = 0.8$). Stress trigger zones appear as warm tones; stress shadows as white (transparent). Increasing time periods after the May shock are used for Figures 11b–11d. Since the first period is truncated 48 days later by the May shock, the full 48-day interval is shown in Figure 11a. Along-fault shocks are gray.

the March rupture but falls under a stress shadow in May, at which time the observed and modeled seismicity rate drops by 40%.

4.3. Model Comparison With Spatial Distribution of Seismicity

[19] Maps of the predicted number of off-fault earthquakes, constructed from the seismicity rate equation, with ΔCFF on east striking receiver faults with $\mu' = 0.8$, are shown in Figure 11. The stress trigger zones appear red because the rate of earthquakes is calculated to exceed the background rate, and the stress shadows appear white (transparent) because the rate of shocks is lower than the background (in other words, few shocks are expected in the shadows). Note that the plots are not cumulative; each earthquake occurs in only one plot. Except for Figure 11a, the time periods are in log time, so there are roughly equal numbers of earthquakes in Figures 11a–11d.

[20] Many of the off-fault seismicity patterns are reflected in the rate/state model. The lobes of predicted off-fault aftershocks following the March main shock roughly correspond with the observed seismicity (Figure 11a). The junction of the May faults lies in a lobe of expected off-

fault seismicity. This pattern is altered by the May main shock (Figure 11b), the fault end lobes from the March shock disappearing and a new lobe extending south from the southern end of the May rupture. With time, the new off-fault lobes grow in intensity and expand away from the fault ruptures, and a memory of the March fault end lobes also becomes apparent.

[21] The calculations in Figure 11 underpredict the number of shocks in the southern lobe and overpredict the number in the northernmost lobe, perhaps because we use a spatially uniform seismicity background rate. Further, the western off-fault seismicity extends to the south of our predicted location. These misfits are reflected in a spatial regression of the observations on the predicted number of earthquakes, in which the along-fault seismicity (gray shocks in Figure 11; also shown in the Figure 10 insets) is excluded. The regression yields $y = 0.74b + 0.27$, with a correlation coefficient $r = 0.27$, for 1674 observations measured in 1 km^2 bins. Here, y is the observed earthquake density, b is the predicted density, and r is the regression coefficient (a perfect correlation would yield $y = 1.0b + 0.0$, with $r = 1.0$). Although the regression is significant at the 99.9% confidence level, it explains only a quarter of the
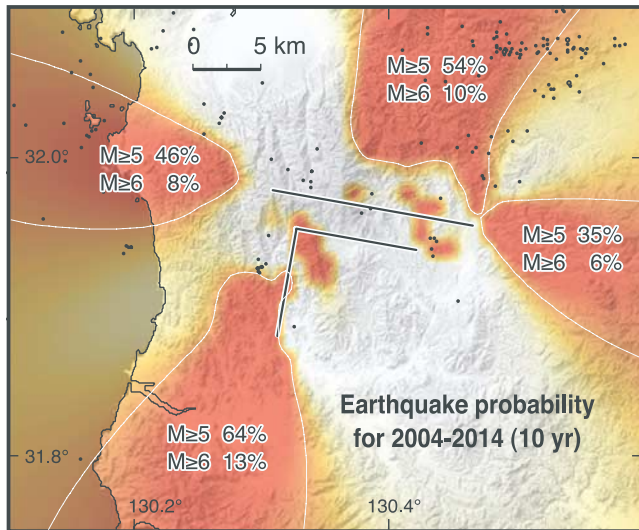
Figure 12. Probability of $M \geq 5$ and $M \geq 6$ shocks in the vicinity of the 1997 Kagoshima earthquake sequence, for the decade, 2004–2014, assuming $A\sigma = 0.4$ bar and $t_a = 20$ years. Probabilities correspond to the areas inscribed by the white lines; the probability is very low in the white regions.

variance in the data. For $\mu' = 0.0$, the observed $r = 0.20$. By comparison, $r = 0.49$ for a study of the 7000 $M \geq 3$ earthquakes that struck during the 2000 Izu Islands swarm [*Toda et al.*, 2002].

4.4. Probability of Future Large Shocks

[22] Given a magnitude-frequency relation, one can easily transform maps of the expected number of $M \geq 0.9$ shocks into the number of earthquakes of any magnitude for any time period. For large events, in which the expected number in a period of interest may be less than one, one can calculate the probability of occurrence in addition to the rate. In our case (Figure 4), the rate of $M \geq 5.0$ shocks is 2.7×10^{-4} times that of $M \geq 0.9$ shocks, and the rate of $M \geq 6$ shocks is 9×10^{-5}. For a stationary Poisson process, the probability, $P = 1 - \exp(-N)$, where N is the number of expected events in a time interval and location of interest. In the four triggering lobes, the 10-year (2004–2014) probability of $M \geq 5$ shocks ranges over 35–64%; for $M \geq 6$ shocks it is 8–13% (Figure 12). For the entire area, there is a 98% probability of $M \geq 5$ (4 shocks expected) and 39% probability of $M \geq 6$ (0.5 shocks expected). Because the correlation coefficient of the observed on predicted $M \geq 0.9$ seismicity (Figure 11d) is low, the true uncertainty on these probabilities is large, and we offer them more as an example rather than a forecast.

[23] Our predicted rate of $M \geq 5$ and $M \geq 6$ shocks for 2004–2014 is 8–17 times higher than the observed back-

ground rate, with all of the increase coming from the trigger zones of Figure 12. Even though there are roughly equal areas of stress increase and decrease, in rate/state stress transfer the exponential response of the seismicity rate to a stress change means that net earthquake rates will be elevated during the aftershock duration. (To gauge the background rates, we use the JMA catalog, which is complete to $M = 5.0$ since 1926, and the Usami catalog, complete to $M = 6.0$ since 1885 [*Usami*, 1996; *Earthquake Research Committee*, 1998]. The rate within the area of Figure 12 is so low that we measure the background rate over a colocated box four times larger, as listed in Table 1.)

5. Discussion and Conclusion

[24] We provide a roadmap to advance from coseismic slip to stress change, from there to time-dependent seismicity, and finally to earthquake probability. Whether others will want to go down this road remains to be seen. The guiding principle is to use the large sample of small earthquakes to test the predicted temporal and spatial distribution of seismicity predicted by rate/state friction. We have met with some progress in this effort, enough perhaps to warrant additional work, but not enough to claim success.

5.1. Uncertainties

[25] We benefited from well-recorded, geometrically simple earthquakes that are close enough to interact strongly. There are nevertheless considerable sources of uncertainty. For the earthquake stress changes (Figure 6), these include the slip model, the friction coefficient, the depth dependence of stress, and the orientation and rake of the assumed receiver planes. For the density plots (Figure 11), additional uncertainties arise from the rate/state parameters, including the aftershock duration, and the assumed spatially uniform values of $A\sigma$ and background seismicity rate r. Finally, for probability forecasts (Figure 12), we further assume that a frequency-magnitude relation derived from the past 5 years applies to the succeeding decade.

5.2. Seismicity Toggling and Dynamic Stress Changes

[26] Most unequivocally, we show that stress changes can turn seismicity on or off. This is important not only to demonstrate the role of static stress changes, but also to argue that the promotion of seismicity by dynamic stress changes is secondary. The dynamic Coulomb stress changes, while spatially nonuniform, everywhere oscillate between positive and negative values [*Kilb et al.*, 2000; *Gomberg et al.*, 2001, 2003]. Thus all regions sustain transient stress increases, and so sudden seismicity rate declines should not be observed. In addition, the dynamic Coulomb stresses are expected to be greatest in the direction of rupture propagation. The March event ruptured largely to the west [*Horikawa*, 2001] and so off-fault seismicity would

Table 1. Background Earthquake Rate in the Kagoshima Region Before May 1997

Earthquake Magnitude	Time Period for Complete Catalog	Observed Number of Shocks	Rate per Decade, km^{-2}	Background Rate per Decade for Area of Figure 12	Predicted for Decade 2004–2014
$M \geq 5$	1926–1997	7	1.25×10^{-4}	0.23	4
$M \geq 6$	1885–1997	3	3.42×10^{-5}	0.06	0.5

be more vigorous to the west if it were promoted by the dynamic stresses (Figure 11d), as is observed. However, the high rate of western off fault seismicity did not occur until long after the May main shock (Figure 6), which ruptured unilaterally to the east and south. Further, there is no eastern off-fault seismicity following the May shock despite an eastward rupture direction, a feature we attribute the static stresses imposed by the March event (Figures 11b–11d). On the basis of a spring-slider dynamic system including inertia and rate/state friction, *Belardinelli et al.* [2003] argue that dynamic stress changes can only promote instantaneous failure, whereas the static stress changes can cause delayed failure, consistent with our observations. However, we do not reproduce the along-fault seismicity in any of these calculations, which we believe arises from stress and geometrical discontinuities that are not included in our smooth slip model. Our ability to consider these shocks must await higher resolution of variable-slip source models, which will surely come.

5.3. Secondary Aftershock Triggering

[27] It is difficult to distinguish an aftershock triggered directly by the main shock stress increase from a secondary aftershock triggered by a preceding aftershock [*Felzer et al.*, 2002]. Rate/state stress transfer also offers insight into the triggering of aftershocks by preceding aftershocks. In Figure 9a, the black line shows an expected tenfold increase in seismicity rate at a site that experienced a 1-bar stress increase. Now assume that an aftershock triggered by this stress increase subjects a much more localized region to an additional 1-bar gain in its trigger zones, and a stress drop in its shadow zones. What happens? Because the main shock increased the seismicity rate over the background rate, the second stress jump causes a 100-fold increase in the seismicity rate over the background, ten times more than the first 1-bar jump. Conversely, even a small stress decrease causes the seismicity in the localized zone to all but stop. This is illustrated by Figure 9b, where a decrease of 1/3 of the preceding increase causes the seismicity rate to drop by three orders of magnitude. Thus the initial stress imparted by the main shock has a lasting effect on subsequent seismicity and is not erased. Secondary aftershocks strongly—but only locally—modify the seismicity set up by the main shock. Ideally, one would include the stress changes associated with decreasingly small aftershocks in a forecast model, but for this one would need reliable source models for the small shocks, which are rarely available.

5.4. Summary

[28] We have argued that the final state of seismicity cannot be calculated by adding the stress contributed by a sequence of earthquakes for two reasons: According to the theory of rate/state friction, the effect of stress on seismicity fades with time, and the stress changes amplify (if positive) or suppress (if negative) the background seismicity rates. The effect of the subsequent stress change on seismicity strongly depends on the seismicity rate (a manifestation of the state variable) immediately beforehand. The theory exhibits a rough match to the distribution, temporal evolution, and apparent migration of the off-fault seismicity at Kagoshima. We found that stress trigger zones enhance seismicity and stress shadows inhibit earthquake occur-

rence. As the observation period approaches the aftershock duration, both the lobes and shadows will fade, but the trigger zones will have produced many more shocks than are missing from the shadows.

References

Belardinelli, M. E., M. Cocco, O. Coutant, and F. Cotton, Redistribution of dynamic stress during coseismic ruptures: Evidence for fault interaction and earthquake triggering, *J. Geophys. Res.*, *104*, 14,925–14,945, 1999.

Belardinelli, M. E., A. Bizzarri, and M. Cocco, Earthquake triggering by static and dynamic stress changes, *J. Geophys. Res.*, *108*(B3), 2135, doi:10.1029/2002JB001779, 2003.

Cocco, M., and J. R. Rice, Pore pressure and poroelasticity effects in Coulomb stress analysis of earthquake interactions, *J. Geophys. Res.*, *107*(B2), 2030, doi:10.1029/2000JB000138, 2002. (Corrrection to "Pore pressure and poroelasticity effects in Coulomb stress analysis of earthquake interactions," *J. Geophys. Res.*, *108*, 10.1029/2002JB002319, 2003.)

Dieterich, J., A constitutive law for rate of earthquake production and its application to earthquake clustering, *J. Geophys. Res.*, *99*, 2601–2618, 1994.

Earthquake Research Committee, *Seismic Activity in Japan: Regional Perspectives on the Characteristics of Destructive Earthquakes*, 222 pp., Sci. and Technol. Agency, Tokyo, 1998.

Felzer, K. R., T. W. Becker, R. E. Abercrombie, G. Ekström, and J. R. Rice, Triggering of the 1999 M_w 7.1 Hector Mine earthquake by aftershocks of the 1992 M_w 7.3 Landers earthquake, *J. Geophys. Res.*, *107*(B9), 2190, doi:10.1029/2001JB000911, 2002.

Fujiwara, S., H. Yarai, S. Ozawa, M. Tobita, M. Murakami, H. Nakagawa, and K. Nitta, Surface displacement of the March 26, 1997 Kagoshima-ken-hokuseibu earthquake in Japan from synthetic aperture radar interferometry, *Geophys. Res. Lett.*, *25*, 4541–4544, 1998.

Gomberg, J., P. A. Reasenberg, P. Bodin, and R. A. Harris, Earthquake triggering by seismic waves following the Landers and Hector Mine earthquakes, *Nature*, *411*, 462–466, 2001.

Gomberg, J., P. Bodin, and P. A. Reasenberg, Observing earthquakes triggered in the near field by dynamic deformations, *Bull. Seismol. Soc. Am.*, *93*, 118–138, 2003.

Guatteri, M., P. Spudich, and G. C. Beroza, Inferring rate and state friction parameters from a rupture model of the 1995 Hyogo-ken Nanbu (Kobe) Japan earthquake, *J. Geophys. Res.*, *106*, 26,511–26,521, 2001.

Harris, R. A., and R. W. Simpson, Supresion of large earthquakes by stress shadows: A comparison of Coulomb and rate-and-state, *J. Geophys. Res.*, *103*, 24,439–24,451, 1998.

Horikawa, H., Earthquake doublet in Kagoshima, Japan: Rupture of asperities in a stress shadow, *Bull. Seismol. Soc. Am.*, *91*, 112–127, 2001.

Hubert-Ferrari, A., A. Barka, E. Jacques, S. S. Nalbant, B. Meyer, R. Armijo, P. Tapponnier, and G. C. P. King, Seismic hazard in the Marmara Sea region following the 17 August 1999 Izmit earthquake, *Nature*, *404*, 269–273, 2000.

Kilb, D., J. Gomberg, and P. Bodin, Earthquake triggering by dynamic stresses, *Nature*, *408*, 570–574, 2000.

Marone, C., Stressed to a quaking point, *Nature*, *419*, 32, 2002.

Matthews, M. V., and P. A. Reasenberg, Statistical methods for investigating quiescence and other temporal seismicity patterns, *Pure Appl. Geophys.*, *126*, 357–372, 1988.

Miyake, H., T. Iwata, and K. Irikura, Strong motion simulation and source modeling of the Kagoshima-ken Hokuseibu earthquakes of March 26 (M_{JMA} 6.5) and May 13 (M_{JMA} 6.3), using empirical Green's function method, *J. Seismol. Soc. Jpn.*, *51*, 431–442, 1999.

Miyamachi, H., K. Iwakiri, H. Yakiwara, K. Goto, and T. Kakuta, Fine structure of aftershock distribution of the 1997 Northwestern Kagoshima earthquakes with a three-dimensional velocity model, *Earth Planets Space*, *51*, 233–246, 1999.

Nalbant, S. S., A. Hubert, and G. C. P. King, Stress coupling between earthquakes in northwest Turkey and the north Aegean sea, *J. Geophys. Res.*, *103*, 24,469–24,486, 1998.

NIED Staff, Seismic moment tensor catalogue, technical note, pp. 205–218, Natl. Res. Inst. for Earth Sci. and Disaster Prevent., Ibaraki, Japan, 2001.

Okada, Y., Internal deformation due to shear and tensile faults in a half-space, *Bull. Seismol. Soc. Am.*, *82*, 1018–1040, 1992.

Parsons, T., R. S. Stein, R. W. Simpson, and P. A. Reasenberg, Stress sensitivity of fault seismicity: A comparison between limited-offset oblique and major strike-slip faults, *J. Geophys. Res.*, *104*, 20,183–20,202, 1999.

Parsons, T., S. Toda, R. S. Stein, A. Barka, and J. H. Dieterich, Heightened odds of large earthquakes near Istanbul: An interaction-based probability calculation, *Science*, *288*, 661–665, 2000.

Reasenberg, P. A., and R. W. Simpson, Response of regional seismicity to the static stress change produced by the Loma Prieta earthquake, *U.S. Geol. Surv. Prof. Pap.*, *1550-D*, 49–72, 1997.

Sagiya, T., S. Miyazaki, and T. Tada, Continuous GPS array and present-day crustal deformation of Japan, *Pure Appl. Geophys.*, *157*, 2303–2322, 2000.

Stein, R. S., The role of stress transfer in earthquake occurrence, *Nature*, *402*, 605–609, 1999.

Stein, R. S., A. A. Barka, and J. H. Dieterich, Progressive failure on the North Anatolian fault since 1939 by earthquake stress triggering, *Geophys. J. Int.*, *128*, 594–604, 1997.

Toda, S., and R. S. Stein, Response of the San Andreas fault to the 1983 Coalinga-Nuñez earthquakes: An application of interaction-based probabilities for Parkfield, *J. Geophys. Res.*, *107*(B6), 2126, doi:10. 1029/2001JB000172, 2002.

Toda, S., R. S. Stein, P. A. Reasenberg, and J. H. Dieterich, Stress transferred by the $M_w = 6. 5$ Kobe, Japan, shock: Effect on aftershocks and future earthquake probabilities, *J. Geophys. Res.*, *103*, 24,543–24,565, 1998.

Toda, S., R. S. Stein, and T. Sagiya, Evidence from the A.D. 2000 Izu Islands swarm that seismicity is governed by stressing rate, *Nature*, *419*, 58–61, 2002.

Usami, T., *Materials for Comprehensive List of Destructive Earthquakes in Japan*, rev. and enlarged ed., 493 pp., Univ. Tokyo Press, Tokyo, 1996.

Wiemer, S., A software package to analyse seismicity: ZMAP, *Seismol. Res. Lett.*, *72*, 373–382, 2001.

Wiemer, S., and M. Wyss, Minimum magnitude of completeness in earthquake catalogs: Examples from Alaska, the western United States, and Japan, *Bull. Seismol. Soc. Am.*, *90*, 859–869, 2000.

Wyss, M., and S. Wiemer, Change in the probability for earthquakes in southern California due to the Landers magnitude 7.3 earthquake, *Science*, *290*, 1334–1338, 2000.

————————————

R. Stein, U.S. Geological Survey, 345 Middlefield Rd, MS 977, Menlo Park, CA 24025, USA. (rstein@usgs.gov)

S. Toda, Active Fault Research Center, Geological Survey of Japan, AIST, Site 7, Higashi 1-1, Tsukuba, Ibaragi-ken 305-8567, Japan. (s-toda@aist.go.jp)